Journal of Alloys and Compounds 523 (2012) 155–160

Contents lists available at SciVerse ScienceDirect

Journal of Alloys and Compounds

journal homepage: www.elsevier.com/locate/jallcom

Complementary information on CdSe/ZnSe quantum dot local structure from extended X-ray absorption fine structure and diffraction anomalous fine structure measurements

E. Piskorska-Hommel[a,b,*], V. Holý[c], O. Caha[d], A. Wolska[b], A. Gust[a], C. Kruse[a], H. Kröncke[a], J. Falta[a], D. Hommel[a]

[a] Institute of Solid State Physics, University of Bremen, Bremen, Germany
[b] Institute of Physics, Polish Academy of Sciences, Warsaw, Poland
[c] Department of Condensed Matter Physics, Charles University in Prague, Czech Republic
[d] Institute of Condensed Matter Physics, Masaryk University, Brno, Czech Republic

ARTICLE INFO

Article history:
Received 13 October 2011
Accepted 24 January 2012
Available online 2 February 2012

Keywords:
CdSe
Quantum dots
EXAFS
DAFS

ABSTRACT

The extended X-ray absorption fine structure (EXAFS) and diffraction anomalous fine structure (DAFS) have been applied to investigate a local structure for the CdSe/ZnSe quantum dots grown by molecular beam epitaxy (MBE) and migration-enhanced epitaxy (MEE). The aim was to study the intermixing of Cd and Zn atoms, chemical compositions and strain induced by cap-layer. The EXAFS at the Cd K-edge and DAFS at the Se K-edge proved the intermixing of Cd and Zn atoms. The distances Cd–Se (2.61 Å) found from EXAFS and DAFS analysis for h_1 region is closer to that in bulk CdSe (2.62 Å). The DAFS analysis revealed the differences in the local structure in two investigated regions (i.e. different iso-strain volumes) on the quantum dots. It was found that the investigated areas differ in the Cd concentration. To explain the experimental results the theoretical calculation based on a full valence-force field (VFF) model was performed. The theoretical VFF model fully explains the experimental data.

1. Introduction

CdSe quantum dots (QDs) in a ZnSe matrix are well studied because of their basic optical and electrical properties [1–3]. The former interest in the 90s was connected with short wavelength light emitters and the realization of a quantum dot laser diode was reported [4]. Recently CdSe QDs gained a new interest as sources for single photon emitters operating at room temperature [5,6]. In contrast to classical III–V materials like InAs/GaAs the formation of CdSe QDs differs significantly from the well-known Stranski–Krastanov growth mode [7]. Either a segregation driven process based on a Cd–Zn exchange is responsible for the CdSe dot formation [8,9] or special temperature ramps have to be applied during the growth to obtain stable CdSe quantum dots [10].

Phenomena based on the introduced strain during epitaxial growth are the driving force for the formation of semiconductor quantum dots. The knowledge of the strain field is a key issue in understanding the mechanisms of the dot formation and their position correlation. CdSe dots and their stacks have been already studied by grazing incidence diffraction (GID) and grazing incidence small angle X-ray scattering (GISAXS) giving detailed information about their structural properties and ordering phenomena [11–13]. The strong intermixing in CdSe/ZnSe structure was found [14–16]. The photoluminescence studies proved the presence of quantum dots; nevertheless, this method cannot give any information about structural properties. Element sensitive transmission electron microscopy (TEM) studies gave a first estimation of the degree of intermixing between the CdSe and the surrounding ZnSe layers [17]. Moreover, the high resolution TEM (HRTEM) figures the depth distribution of Cd in CdSe/ZnSe structure.

These kinds of information are hardly possible to gain from high-resolution X-ray diffraction (HRXRD) due to the small scattering volume of CdSe quantum dots. However, grazing incidence X-ray diffraction (GID) provides structural knowledge despite small volume scattering, since the penetration depth of the incoming X-ray beam is comparable to the size of the nanostructures. Nevertheless the understanding of the local structure of the quantum dots themselves and their environment is still rudimentary.

Since EXAFS method is sensitive to the local structure around a selected atom, it is suitable to give quantitative local structure information [18,19]. On the other hand, the application of EXAFS to the investigation of nanostructures is rather limited, since the

* Corresponding author at: Institute of Solid State Physics, University of Bremen, Bremen, Germany.
E-mail address: e.piskorska@ifp.uni-bremen.de (E. Piskorska-Hommel).

0925-8388/$ – see front matter © 2012 Elsevier B.V. All rights reserved.
doi:10.1016/j.jallcom.2012.01.133

measured signal is averaged over the sample volume, i.e. it is hardly possible to get separately the information from the substrate, the quantum structure and the cap layer. The local structural information from quantum dots can be obtained using diffraction anomalous fine structure (DAFS) in grazing-incidence (GI) geometry that combines the X-ray absorption and diffraction methods. The advantage of the DAFS method is that the diffracted intensity is measured as a function of X-ray energy close to the absorption edge [20,21]. Thus, in contrast to the volume-averaged EXAFS signal, the DAFS signal is collected from a volume with a given lattice-plane distance, i.e. with a given strain (iso-strain volume).

The EXAFS and DAFS techniques were successfully applied to various semiconductor systems [22–24]; however, to our knowledge, no simultaneous EXAFS/DAFS study has been carried out on CdSe quantum dots grown by molecular beam epitaxy (MBE) and migration-enhanced epitaxy (MEE). Therefore, we took advantage of abilities both EXAFS and DAFS techniques, and used them to probe the fine structure of the Cd and Se K-absorption edges.

Epitaxial grown sandwich structures are distorted by strain originating from the mismatch of the crystal lattices involved. We have simulated the bond lengths in a strained $Cd_xZn_{1-x}Se$ dot lattice of the quantum dots, using both the original valence-force field (VFF) model [25–28] and a simplified approach taking into account small strained $Cd_xZn_{1-x}Se$ random clusters [29–31]. From the simulations we obtained the Zn–Se and Cd–Se bond-lengths for various strains in the dot lattice and we compared the simulation results with the EXAFS and DAFS data.

In the presented paper we report the results of a comprehensive investigation of the local atomic structure in CdSe/ZnSe quantum dots grown by MBE and MEE methods in order to understand the dot formation process.

2. Experimental procedure and data analysis

The studied CdSe/ZnSe single quantum dots layers were grown at 280 °C on GaAs (0 0 1) substrates by molecular beam epitaxy (MBE) equipped with Zn, Cd and Se elemental sources for II–VI layer growth. The CdSe monolayers (3 ML) were deposited by migration-enhanced epitaxy (MEE) and embedded in a 1.4 nm ZnSe layer with 50 nm thick ZnSe underneath and 25 nm above this dot structure. The existence of the CdSe quantum dots, which form during the overgrowth process, was proved by time-resolved photoluminescence spectroscopy (PL) [9].

Both, EXFAS and DAFS data were collected at the European Synchrotron Radiation Facility (ESFR), Grenoble, France.

The EXAFS spectra at the Cd K edge (~27 keV) were collected at fluorescence mode using a multi-element Ge detector at the Grenoble Italian beamline for Diffraction and Absorption (GILDA) Collaborating Researcher Group (CRG) beamline.

The DAFS spectra at the Se K-edge (~12.7 keV) were collected at the beamline BM02, in grazing-incidence geometry at different positions in reciprocal space near the (8 0 0) diffraction spot (for various deviations q_r from the reciprocal lattice point) in order to obtain local chemical information and information on the atomic ordering in a particular iso-strain volume. The q_r axis was chosen along the (h 0 0) line (radial direction). The DAFS signal stems from an iso-strain volume, the position of which is determined by the value of the q_r coordinate, where the DAFS signal was collected. The grazing incidence geometry allowed us to reduce the contribution of the substrate to the scattered intensity and enhances the contribution of the quantum dots to the measured signal. To avoid the oxidation, the samples were kept in He atmosphere during the measurement.

The Athena program was used to subtract the pre-edge background, to normalize to the experimental edge step and absorption data from the EXAFS data [32].

The DAFS spectrum $\chi(E)$ depends on the real (χ') and imaginary (χ'') parts of the anomalous form-factor of the Se atoms. The numerical Kramers–Kronig transformation was used to extract the imaginary part $\chi''(E)$ of the DAFS spectrum according the expression described in detail in Ref. [33]. Since the investigated quantum dots are extremely small, the DAFS signal is rather weak and the noise level is high. Therefore, we used an optimized smoothing procedure based on smoothing splines of the 4th order to filter out the random noise in the $\chi(E)$ spectra.

The smoothed DAFS oscillations were Fourier transformed to the real space (R-space). Both EXAFS and DAFS data were fitted in R-space to obtain the structure parameters, i.e., bond lengths (R), Debye–Waller factors (σ^2) and coordination numbers (N) using Artemis program [34]. The theoretical scattering paths were generated by the FEFF 8 code for the Cd–Se, Cd–Cd and Cd–Zn pairs [35].

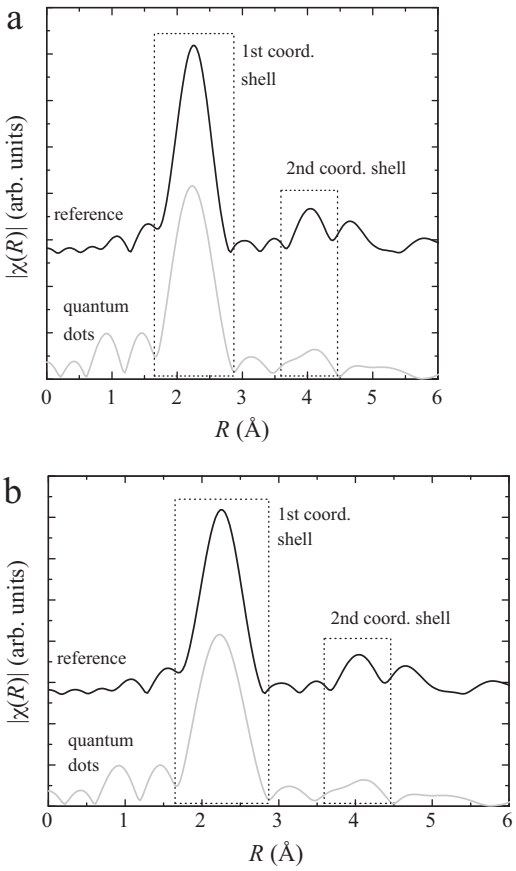

Fig. 1. The k-weighted EXAFS oscillations $k\chi(k)$ (a) and (b) the magnitude of the Fourier transformation for the reference sample CdSe and investigated CdSe/ZnSe quantum dots at the Cd K-edge at the Cd K-edge for references and investigated samples: CdSe and CdSe quantum dots.

3. Results

3.1. EXAFS on the Cd K-edge

The comparison of the EXAFS oscillations and their representative Fourier transforms to real space for the Cd K-edge for the bulk CdSe and studied CdSe/ZnSe quantum dots is presented in Fig. 1a and b, respectively. From the qualitative analysis one can see that the number of oscillations for quantum dots and the bulk CdSe is similar. But the oscillations for studied sample are shifted to larger k compared to the bulk sample, indicating some disorder in the examined sample. The second coordination shell between 3.5 and 4.5 Å visible in Fig. 1b is broader for the studied samples in comparison to the bulk one, giving evidence for the existence of more than one species' of atoms in this shell. The Fourier transform of the EXAFS oscillations of CdSe/ZnSe quantum dots and the best fitting results of the two coordination shells are shown in Fig. 2. The fitting analysis was carried out in the range of k = 3–10 Å^{-1} and R = 1.4–4.6 Å using the Kaiser–Bessel window. The resulting structural parameters for investigated and reference CdSe sample are listed in Table 1. The first coordination shell in the samples under examination is composed by 4 Se near-neighbors, while the second one by a mixture of Cd and Zn. Their coordination number is kept 12 as follows from the nominal zinc-blende lattice. From the quantitative analysis the Cd–Se bond length was determined as 2.61 Å. The next-neighbor distance Cd–Cd in the second coordination shell is larger by about 0.06 Å from that in the pure CdSe compound (4.31 Å), whereas the bond length Cd–Zn was found to

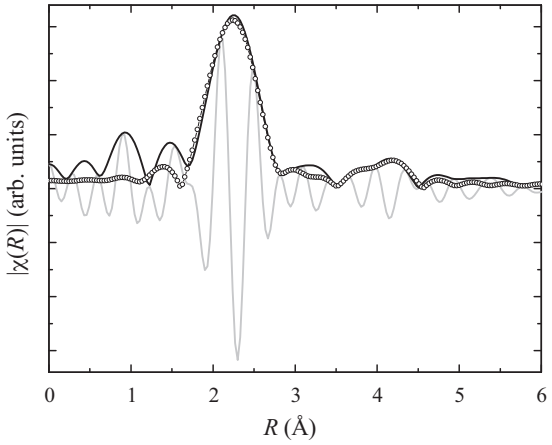

Fig. 2. The magnitude (black line) and the real part (grey line) of the Fourier transformation of the EXAFS oscillations presented in Fig. 1 and the best fit (circles) of the first and second coordination shells for CdSe quantum dots.

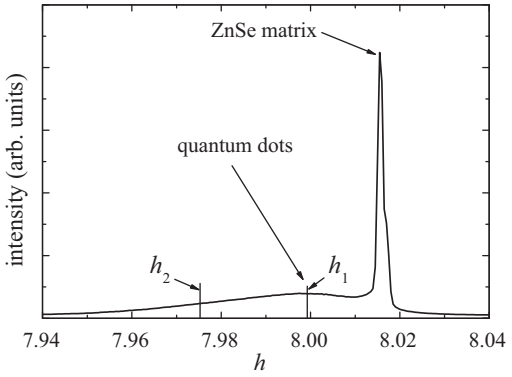

Fig. 3. The diffraction profile measured in radial (8 0 0) direction. The h_1 and h_2 indicate the radial positions in reciprocal space where the DAFS data were collected.

be 4.18 Å. The value of the Debye–Waller factor for distances Cd–Se and Cd–Cd is similar to this found for reference CdSe compound.

3.2. DAFS on the Se K-edge

The diffraction profile in the radial (8 0 0) direction is shown in Fig. 3. The h_1 and h_2 indicate the radial positions in reciprocal space on the quantum dots where the DAFS spectra shown in Fig. 4 were collected. The presented data are an average of 15 scans. In spite of

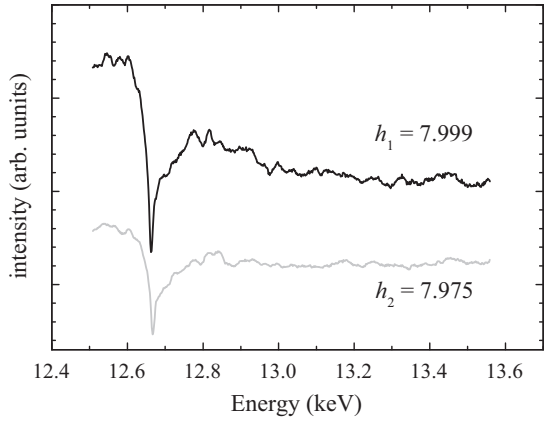

Fig. 4. Raw DAFS spectra collected at the Se K-edge at two different values of h indicated in Fig. 3.

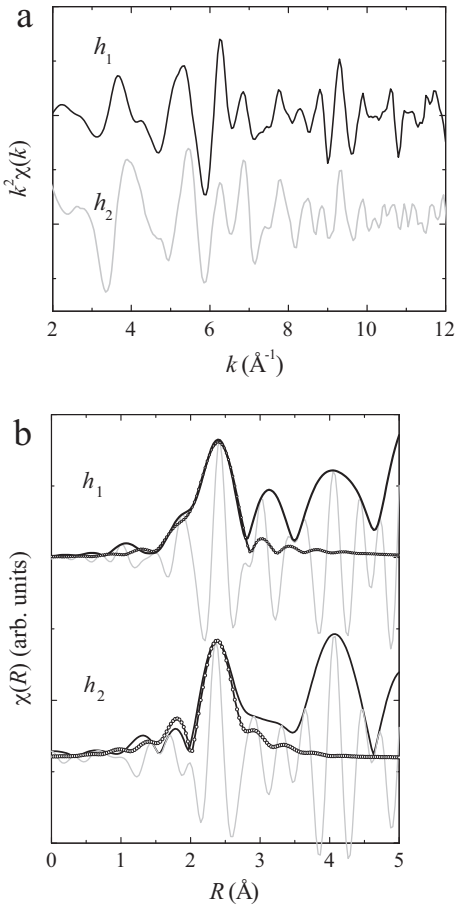

Fig. 5. (a) The oscillations extracted from the DAFS spectra plotted in Fig. 4; (b) the magnitude (black line) and real part (grey line) of the Fourier transform of the k^2-weighted oscillations recorded at positions h_1 and h_2. The data (solid line) and their best fit (circles) of the first coordination shell in CdSe quantum dots are shown.

the worse quality of the DAFS data compared to EXAFS results (due extreme stability requirements of the DAFS method and a very low diffracted intensity) we were able to use the data for the determination of the first coordination shell around the Se atoms. It was not possible to determine the radii of higher coordination shells, since smoothed $\chi(E)$ spectra used in the Kramers–Kronig analysis do not contain higher frequencies necessary for the calculation of the $\chi(R)$ values for larger R.

The oscillations extracted from the DAFS spectra for the Se K-edge for different h values, their Fourier transform and the best fitting results of the first coordination shell are shown in Fig. 5a and b, respectively. The peak positioned at 2.4 Å (without phase correction) in the Fourier transform and presented in Fig. 5b corresponds to the first coordination shell which is a mixture of Cd and Zn atoms. The small peaks between 1 and 2 Å and the peaks beyond the first coordination shell in the Fourier-transformed data correspond to a combination of a residual background, noise and a truncation error. Luck higher coordination shell can suggest very small size of the formed nano-objects. It is remarkable that the oscillations derived from two different h values are mutually phase shifted. This fact can indicates a difference in the local structure in various iso-strain volumes corresponding to the points h_1 and h_2.

The quantitative analysis was done in the photoelectron wave vector range of $k = 3–11$ Å^{-1} and $R = 1.4–2.8$ Å (i.e. only the first coordination shell was fitted) and the results are summarized in Table 1. The Se–Cd distances are 2.62 Å and 2.54 Å for position on the quantum dots h_1 and h_2, respectively. The Zn–Se bond lengths were

Table 1
The EXAFS and DAFS fitting results determined for Cd and Se K-edge, respectively. R are the distances between the absorbing atom and its near-neighbors, N is the coordination number, σ^2 is the Debye–Waller factor, respectively.

	EXAFS (Cd K-edge; 2 shells)		DAFS (Se K-edge; one shell)	
	CdSe	Sample	h_1	h_2
N_{Se}	4	4	–	–
N_{Cd}	12	5(2)	1.6 (0.4)	2.8 (0.8)
N_{Zn}	–	7(2)	2.4 (0.4)	1.2 (1)
R_{Cd-Se} (Å) (2.62)	2.62 (0.01)	2.61 (0.01)	2.62 (0.02)	2.54 (0.03)
R_{Cd-Cd} (Å) (4.28)	4.31 (0.02)	4.37 (0.02)	–	–
R_{Cd-Zn} (Å) (4.01)	–	4.18 (0.04)	–	–
R_{Se-Zn} (Å) (2.45)	–	–	2.45 (0.02)	2.45 (0.03)
σ^2_{Cd-Se} (Å^2)	0.003 (0.001)	0.002 (0.001)	0.004 (0.002)	0.009 (0.003)
σ^2_{Cd-Cd} (Å^2)	0.014 (0.002)	0.012 (0.005)	–	–
σ^2_{Cd-Zn} (Å^2)	–	0.015 (0.003)	–	–
σ^2_{Se-Zn} (Å^2)	–	–	0.008 (0.005)	0.023 (0.009)

found at 2.45 Å and 2.48 ± 0.01 Å, for both position, namely for h_1 and h_2.

4. Theoretical model

In literature, two models that describe the structure of ternary compounds are reported. One is based on the virtual crystal approximation; the second one assumes a random solid solution [31,36,37]. The former approach assumes that all atoms occupy the average lattice positions and the lattice parameters change linearly with the composition [37]. In the latter the distances anion–cation in the first shell are close to those in the binary system [30,31], but the distances in coordination shell beyond first follow the virtual crystal approximation (VCA) model [37]. The numerical simulations of the bond lengths presented in this section go beyond these approximations. In particular we use a full valence-force field model (VFF) [28]. In this model we considered a $Cd_xZn_{1-x}Se$ crystal domain with $15 \times 15 \times 15$ elementary unit cells and periodic boundary conditions. Using a random generator, we defined the positions of Cd and Zn cations in the lattice for a given Cd concentration x. For a given microscopic distribution of cations we minimized the lattice energy using the standard VFF-model expression in Ref. [26], determining the coordinates of all atoms in the domain. In order to obtain statistically averaged results, we performed the minimization many times for various microscopic distributions of the cations and the same Cd content x. The whole simulation procedure was carried out for two strain statuses of the dot lattice, namely (a) for a fully relaxed lattice and (b) for a biaxially strained (pseudomorph) lattice deposited coherently on a GaAs substrate. In the former case, we determined the average lattice parameter of the alloy as well, in the latter we assume that the lateral lattice parameters along [1 0 0] and [0 1 0] equal the lattice parameter of GaAs, the vertical lattice parameter along [0 0 1] was determined by the minimization procedure.

The VFF approach yielded the distributions of the bond lengths of all pairs Zn–Zn, Zn–Cd, Zn–Se, Cd–Cd, Cd–Se, and Se–Se so that its results can be used for the interpretation not only of the DAFS data at the Se K edge but also of the EXAFS spectra at the Cd K absorption edge. As an illustration of the simulation results we present in Fig. 6 the histograms of the relative occurrence $N(R)$ of the Cd–Se and Zn–Se bond lengths calculated for various Cd concentrations x obtained by the exact simulation VFF method and both types of the elastic strain (a) and (b) explained above. It is worthy to note that the distribution of the bond lengths is asymmetric both for small and high Cd concentrations; for $x \approx 0.5$, the distribution of the bond lengths is almost symmetric. In the relaxed lattice, the Cd–Se and Zn–Se bond lengths increase almost linearly with increasing Cd concentration x, in the strained state however the mean bond-lengths of both pair types slightly decrease with increasing x.

5. Discussion

The zinc blende structure in the thin ternary layer was widely studied in the literature. It was found that the strain that accumulates in the structure results in bond-angle distortion and the bond lengths anion–cation remain close to the unstrained values in the binary compound. D'Acapito and Woicik pointed out that the anion–cation bond length varies much more in the relaxed alloy than in the strained ones. Only small variations of the bond length in the strained layer with composition are observed [29,30]. Our theoretical model proved this result, i.e. only small dependence of the anion–cation bond length on the Cd compositions was found. Therefore, if the studied nano-objects in the presented paper are strained the distances Se–Cd and Se–Zn should not change significantly. In the relaxed state, both distances should slightly increase with increasing Cd content [38].

The quantum dot formation reported here differs from the well-known Stranski–Krastanov growth mode. The Zn-induced reorganization of the CdSe layer during the overgrowth process is responsible for the dot formation resulting in the CdSe intermixing with ZnSe. In fact, the quantum dots consist of a ternary CdZnSe compound. The presence of the QDs was proved by PL, TEM [8,9]. It was found that two region with low and high Cd concentration are present.

The EXAFS signal stems from the whole volume of the sample, thereby in an EXAFS experiment it is not possible to discriminate between the dot and substrate volumes, so that the EXAFS signal contains average information from both volumes. Our EXAFS results could not give an obvious answer concerning the details of the local structure in the formed ensemble of quantum dots. We found that the distances Cd–Se are close to these in the binary compound CdSe (2.62 Å). Due to the high uncertainty in the second coordination shell the estimated values from the EXAFS analysis did not allow for the identification of the nature of the bond lengths. One can only conclude that the EXAFS data correspond to a mixture of Cd and Zn and the average Cd content in the studied sample is present around 42%, $x = 0.42$. According to Refs. [29,30] and to our theoretical model, EXAFS results suggest that the formed structure resembles relaxed random $Cd_xZn_{1-x}Se$ alloy.

Opposite to the EXAFS, the DAFS method is more "local" and only the structure within the quantum dots volume was examined by this method. The DAFS analysis shows that the Cd–Se distances 2.62 Å and the Zn–Se distances 2.45 Å in the point h_1 (see Table 1) correspond to the values displayed in Fig. 6 for fully relaxed $Cd_xZn_{1-x}Se$ lattice with x in the range from 0.1 to 0.5. The fairly

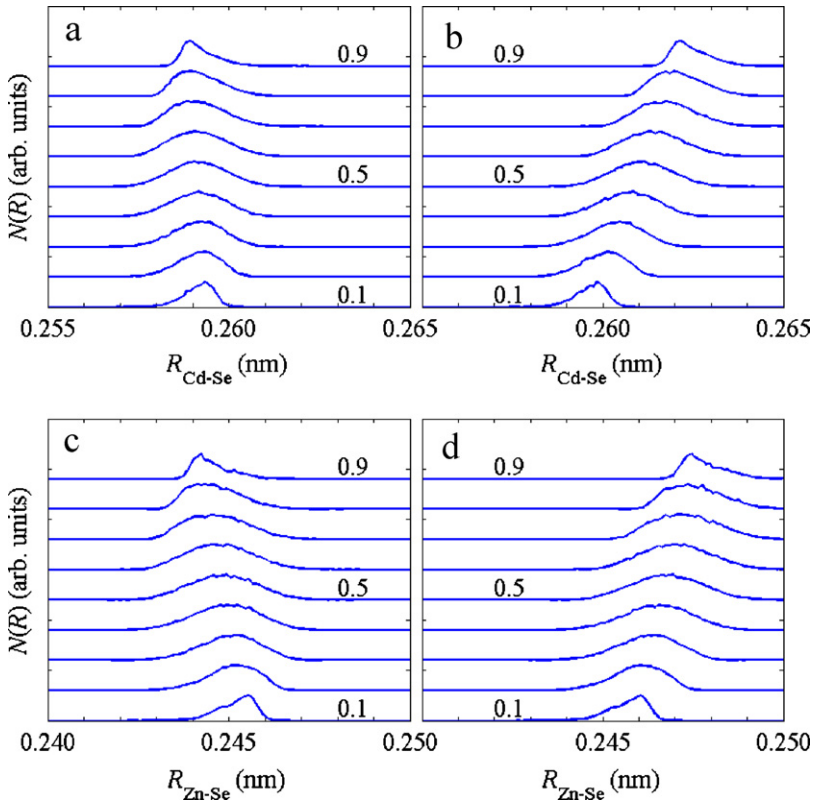

Fig. 6. The distribution of the Cd–Se (a and b) and Zn–Se (c and d) bond lengths calculated by the valence-field model assuming fully relaxed (b and d) and biaxially strained (a and c) $Cd_xZn_{1-x}Se$ lattice (see the text for details). The parameter of the curves is the concentration x of Cd. The curves are shifted vertically for clarity.

low Debye–Waller factor related to Cd–Se and Zn–Se bond lengths pointed out that the region h_1 is well ordered.

The volume connected to the point h_2 cannot be described by a relaxed or strained random alloy, however the distance Se–Zn approaches the bulk value 2.45 Å. The large value of the Debye–Waller factor of the Zn–Se distances indicates that the Zn atoms are irregularly distributed in the studied structure (Table 1). Moreover, almost two times larger Cd content was found in region h_2 than in h_1, namely $x = 0.7$.

The PL results indicate that the mean Cd content in the dot volumes is about 80% ($x = 0.8$). Despite to the high Cd content in point h_2, the Se–Cd bond lengths are shorter by about 0.8 Å from those in the bulk material. From Fig. 6 it follows that in the pseudomorph state the distance Se–Cd only slightly depends on the Cd content, so the strain is not responsible for the shortening the anion–cation distance. The intended thickness of the CdSe layer was around 3 ML (1 ML = 0.287 nm). Nevertheless, approximately 50% deposited CdSe get lost due to cap layer ZnSe grown by MEE method [8]. The short Se–Cd distances indicate small size of the quantum dots. The explanation of the observed discrepancy in the structure studied for two different points is that, the QDs consist of two regions, i.e. a reach-Cd region, which is embedded in a ternary ZnCdSe-compound region. The thickness of the reach-Cd region is around ~1.8 ML.

6. Conclusions

The X-ray absorption and diffraction spectroscopy methods EXAFS and DAFS allowed establishing the nature of the bond lengths in the quantum dots. The analysis showed that an intermixing between Cd and Zn atoms occurs and the Cd content in the volume of the quantum dots varies from ~40% to ~70%. The EXAFS and DAFS analysis provided that the anion–cation Cd–Se bond lengths in the h_1 point correspond to a fully relaxed $Cd_xZn_{1-x}Se$ alloy with x between 0.4 and 0.5. The Cd–Se and Zn–Se bond-lengths of strained and relaxed $Cd_xZn_{1-x}Se$ alloy lattices have been calculated by a valence-force field model and a good correspondence of the measured and calculated data has been achieved. It was found that the QDs grown by MEE method are composed of a reach-Cd region embedded in ZnCdSe region with a lower Cd concentration.

EXAFS and DASF results are consistent with the results obtained by PL, TEM, HRXRD and temperature dependent, time resolved spectroscopy [9].

Acknowledgments

This work was supported in part by the Polish State Committee for Scientific Research (Grant No. N202 142 32/3888) and the German Research Council (DFG project PI 819/1-1). V.H. acknowledges the support from the project MSM0021620834 financed by the Ministry of Education of the Czech Republic. We would like to thank the beamline scientists F. d'Acapito and H. Renevier for help during the experiment.

References

[1] K. Leonardi, H. Heinke, K. Ohkawa, D. Hommel, H. Selke, F. Gindele, U. Woggon, Appl. Phys. Lett. 71 (1997) 1510.
[2] M. Scheibner, T. Schmidt, L. Worschech, A. Forchel, G. Bacher, T. Passow, D. Hommel, Nat. Phys. 3 (2007) 106.
[3] T. Kümmell, R. Weingand, G. Bacher, A. Forchel, K. Leonardi, D. Hommel, H. Selke, Appl. Phys. Lett. 73 (1998) 3105.
[4] M. Klude, T. Passow, R. Kröger, D. Hommel, Electr. Lett. 37 (2001) 1119.
[5] K. Sebald, P. Michler, T. Passow, D. Hommel, G. Barcher, A. Forchel, Appl. Phys. Lett. 81 (2002) 2920.
[6] R. Arians, T. Kümmell, G. Bacher, A. Gust, C. Kruse, D. Hommel, Appl. Phys. Lett. 90 (2007) 101114.

[7] D. Litvinov, A. Rosenauer, D. Gerthsen, P. Kratzert, M. Rabe, F. Henneberger, Appl. Phys. Lett. 81 (2002) 640.
[8] T. Passow, H. Heinke, T. Schmidt, J. Falta, A. Stockmann, H. Selke, P.L. Ryder, K. Leonardi, D. Hommel, Phys. Rev. B 64 (2001) 193311.
[9] T. Passow, K. Leonardi, H. Heinke, D. Hommel, D. Litvinov, A. Rosenauer, D. Gerthsen, J. Seufert, G. Bacher, A. Forchel, J. Appl. Phys. 92 (11) (2002) 6546.
[10] F. Henneberger, M. Rabe, M. Lowisch, F. Henneberger, J. Cryst. Growth 184/185 (1998) 248.
[11] T. Schmidt, T. Clausen, J. Falta, G. Alexe, T. Passow, D. Hommel, S. Bernstorff, Appl. Phys. Lett. 84 (2004) 4367.
[12] T. Schmidt, E. Roventa, T. Clausen, J.I. Flege, G. Alexe, S. Bernstorff, C. Kübel, A. Rosenauer, D. Hommel, J. Falta, Phys. Rev. B 72 (2005) 195334.
[13] T. Passow, H. Heinke, J. Falta, K. Leonardi, D. Hommel, Appl. Phys. Lett. 77 (22) (2000) 3544.
[14] T. Passow, K. Leonardi, A. Stockmann, H. Selke, H. Heinke, D. Hommel, J. Phys. D 32 (1999) A42.
[15] R.N. Kyutt, A.A. Toropov, S.V. Sorokin, T.V. Shubina, S.V. Ivanov, M. Karlsteen, M. Willander, Appl. Phys. Lett. 75 (1999) 373.
[16] N. Peranio, A. Rosenauer, D. Gerthsen, S.V. Sorokin, I.V. Sedova, S.V. Ivanov, Phys. Rev. B 61 (2000) 16015.
[17] D. Litvinov, A. Rosenauer, D. Gerthsen, N.N. Ledentsov, Phys. Rev. B 61 (2000) 16819.
[18] B.K. Teo, EXAFS: Basic Principles and Data-analysis. Springer, New York, 1986.
[19] B.K. Teo, D.C. Joy, EXAS Spectroscopy. Techniques and Applications, 1981.
[20] J.O. Cross, Ph.D. thesis, University of Washington, Seattle, 1996.
[21] A. Létoublon, V. Favre-Nicolin, H. Renevier, M.G. Proietti, C. Monat, M. Gendry, O. Marty, C. Priester, Phys. Rev. Lett. 92 (2004) 186101.
[22] C. Lamberti, Surf. Sci. Rep. 53 (1) (2004), among others.
[23] M.G. Proietti, et al., Phys. Rev. B 59 (1999) 5479.
[24] J. Coraux, et al., Phys. Rev. B 75 (2007) 235312.
[25] J. Martins, A. Zunger, Phys. Rev. B 30 (1984) 6217.
[26] P. Keating, Phys. Rev. 145 (1966) 637.
[27] R.M. Martin, Phys. Rev. B 1 (1970) 4005.
[28] Y. Cai, M.F. Thorpe, Phys. Rev. B 46 (1992) 15872.
[29] F. d'Acapito, J. Appl. Phys. 96 (1) (2004) 369.
[30] J. Woicik, Phys. Rev. B 57 (1998) 6266.
[31] A. Balzarotti, N. Motta, A. Kisiel, M. Zimnal-Starnawska, M. Czyzyk, M. Podgorny, Phys. Rev. B 31 (1985) 7526.
[32] http://cars.uchicago.edu/ifeffit.
[33] I.J. Pickering, et al., J. Appl. Phys. 32 (1993) 32.
[34] B. Ravel, M. Newville, J. Synchrotron Radiat. 12 (2005) 537.
[35] S.I. Zabinsky, J.J. Rehr, A. Ankudinov, R.C. Albers, M.J. Eller, Phys. Rev. B 52 (1995) 2995.
[36] J. Mikkelsen, J.B. Boyce, Phys. Rev. B 28 (1983) 7130.
[37] J.C. Mikkelsen, J.B. Boyce, Phys. Rev. Lett. 49 (1982) 1412.
[38] F. Loglio, A.M. Telford, E. Salvietti, M. Innocenti, G. Pezzatini, S. Cammelli, F. D'Acapito, R. Felici, A. Pozzi, M.L. Foresti, Electrochim. Acta 53 (23) (2008) 6978.